Intermediates in the Reaction of Fully Reduced Cytochrome *c* Oxidase with Dioxygen†

Artur Sucheta, Istvan Szundi, and Ólöf Einarsdóttir*

Department of Chemistry and Biochemistry, University of California, Santa Cruz, California 95064

Received May 11, 1998; Revised Manuscript Received August 12, 1998

ABSTRACT: The reduction of dioxygen to water by cytochrome *c* oxidase was monitored in the Soret region following photolysis of the fully reduced CO complex. Time-resolved optical absorption difference spectra collected between 373 and 521 nm were measured at delay times from 50 ns to 50 ms and analyzed using singular value decomposition and multiexponential fitting. Five processes were resolved with apparent lifetimes of 0.9 μs, 8 μs, 36 μs, 103 μs, and 1.2 ms. A mechanism is proposed and spectra of intermediates are extracted and compared to model spectra of the postulated intermediates. The model builds on an earlier mechanism that used data only from the visible region (Sucheta et al. (1997) *Biochemistry 36,* 554−565) and provides a more complete mechanism that fits results from both spectral regions. Intermediate 3, the ferrous−oxy complex (compound A) decays into a 607 nm species, generally referred to as P, which is converted to a 580 nm ferryl form (F_o) on a significantly faster time scale. The equilibrium constant between P and F_o is 1. We propose that the structure of P is a_3^{4+}═O Cu_B^{2+}−OH^- with an oxidizing equivalent residing on tyrosine 244, located close to the binuclear center. Upon conversion of P to F_o, cytochrome *a* donates an electron to the tyrosine radical, forming tyrosinate. Subsequently a proton is taken up by tyrosinate, forming F_I [a_3^{4+}═O Cu_B^{2+}−OH^- a^{3+} Cu_A^{+}]. This is followed by rapid electron transfer from Cu_A to cytochrome *a* to produce F_{II} [a_3^{4+}═O Cu_B^{2+}−OH^- a^{2+} Cu_A^{2+}].

The nature of the intermediates present during the reduction of dioxygen to water by cytochrome *c* oxidase continues to be a subject of discussion. Time-resolved resonance Raman experiments at room temperature have provided evidence for the formation of a ferrous−oxy complex on a time scale of ∼10 μs (*1*−*3*), the presence of a ferryl (a_3^{4+}═O) between 300 μs and 1.5 ms, and a ferric hydroxide on a millisecond time scale (>0.5 ms) (*4*−*7*). An additional intermediate, usually referred to as P, has been proposed as an intermediate between compound A and the ferryl form (*7*−*11*). This proposal is partially based on results obtained by reversing the dioxygen reduction reaction in energized mitochondria, in which intermediates with maxima at 580 and 607 nm (referenced against the oxidized enzyme) were observed and assigned to a ferryl (F, a_3^{4+}═O Cu_B^{2+}) and a peroxy (P, a_3^{3+}−O^-−O^- Cu_B^{2+})[1] form, respectively (*12*). Species with spectral characteristics similar to those of P and F are also formed upon addition of hydrogen peroxide to the resting state of the enzyme, while a P-like product results from exposure of oxidized enzyme to a mixture of carbon monoxide and oxygen (*13*−*16*). However, until recently (*10, 11*), there was no time-resolved spectroscopic evidence for the 607 nm species being an intermediate during the reduction of dioxygen to water by fully reduced cytochrome oxidase.

The nature of P (hereafter called the 607 nm species) has been under debate, and structures have been proposed in which cytochrome a_3 is in a peroxy form (a_3^{3+}−O^-−O^-) (*10*−*12*, *17*−*19*), a ferryl state (a_3^{4+}═O) with an oxidizing equivalent on an amino acid radical or on Cu_B (Cu_B^{3+}) (*16, 20*), or in a_3^{5+}═O form with Cu_B^{2+} (*21*). Models have also been proposed in which a mixture of two intermediates, peroxy and ferryl, is formed following decay of compound A (*22*−*25*).

We recently used optical multichannel detection to investigate the reaction of fully reduced cytochrome oxidase with dioxygen in the visible region (460−720 nm) following photolysis of the fully reduced CO complex (*11*). Our results suggested that the ferrous−oxy complex (compound A) decayed into a 1:6 mixture of two species, termed P and P′, respectively, in both of which cytochrome a_3 was postulated to be in a peroxy state (a_3^{3+}−O^-−O^-), while cytochrome *a*

† This work was supported by the National Institutes of Health Grant GM53788.

* To whom correspondence should be addressed. Fax: 831-459-2935. E-mail: olof@chemistry.ucsc.edu.

[1] Abbreviations: SVD, singular value decomposition; OSMA, optical spectrometric multichannel analyzer; **b**-spectrum, spectral changes associated with a particular first-order process; **u**-spectra, the orthonormal basis spectra represented by the *n* columns of the **U** matrix from SVD.; **v**-vectors, the *n* columns of the **V** matrix from SVD, describing the time evolution of the corresponding **u**-spectra; τ, apparent lifetime = 1/(rate constant); Cu_A, the mixed-valence copper A center; Cu_B, copper B; a^{2+}, reduced cytochrome *a*; a^{3+}, oxidized cytochrome *a*; a_3^{2+}, reduced cytochrome a_3; a_3^{3+}, oxidized cytochrome a_3; compound A, the ferrous−oxy complex of cytochrome a_3; P, a form of the enzyme in which cytochrome a_3 has an absorbance maximum at ∼607 nm when referenced against its oxidized state; F, a form of the enzyme in which cytochrome a_3 has an absorbance maximum at ∼580 nm when referenced against its oxidized state; F_o, F in which cytochrome *a* is oxidized, one proton is at the binuclear center, and tyrosine is deprotonated; F_I, F in which cytochrome *a* is oxidized, one proton is at the binuclear center, and tyrosine is protonated; F_{II}, F in which cytochrome *a* is reduced, one proton is at the binuclear center and tyrosine is protonated.

10.1021/bi981092w CCC: $15.00
Published on Web 11/26/1998

was reduced in P and oxidized in P′. In both species cytochrome a_3 had an absorption maximum at 606 nm when referenced against its oxidized form, analogous to the model spectrum obtained by adding a mixture of CO and O_2 to the oxidized enzyme. However, despite similarities in the wavelengths of the absorption maxima between the experimental and model spectra, there were significant differences in the shape and bandwidth of the absorption bands (Figure 5d, of ref *11*). This suggests that the intermediate formed upon decay of compound A might be different than the 607 nm species generated upon exposure of the oxidized enzyme to CO in the presence of O_2.

Here we report transient absorbance changes in the Soret region during the reaction of the fully reduced enzyme with dioxygen. We have interpreted the data in terms of a mechanism similar to that proposed previously (*11*) and extracted the spectra and time evolution of the intermediates in both the Soret and visible regions. Significantly, when both the visible and Soret data are taken into account, the spectrum of intermediate 4, which is formed during the decay of compound A, can be satisfactorily modeled by a 1:1 mixture of the 607 and 580 nm species but not by the 607 nm species alone. We propose that the structure of the 607 nm species is a_3^{4+}═O $Cu_B^{2+}-OH^-$ with tyrosine 244 providing a hydrogen atom necessary for the O−O bond cleavage.

MATERIALS AND METHODS

Cytochrome oxidase was isolated from bovine hearts according to the method of Yoshikawa et al. (*26*). The final precipitate was dissolved in 0.1 M sodium phosphate buffer, pH 7.4, and dialyzed overnight against the same buffer. The fully reduced form and fully reduced CO-bound enzyme complex were prepared as described earlier (*11*) using sodium L-ascorbate and ruthenium(II) hexaammine chloride as a reducing agent and mediator, respectively.

The reaction of the fully reduced enzyme with dioxygen was investigated following photolysis of the fully reduced CO complex as previously described (*11*). Briefly, a solution of the fully reduced CO complex in 0.1 M sodium phosphate buffer (pH 7.4), saturated with CO/N_2 (1:9), was mixed in a 1:1 ratio with O_2-saturated buffer (1.25 mM) in a flow apparatus interfaced to a laser photolysis/multichannel detection system. Enzyme concentration, equal to half the heme A concentration, was 4.9 μM after mixing. The photolytic efficiencies in the Soret region measured under identical conditions in the absence of O_2 were ∼73%, resulting in an effective concentration of 3.6 μM. The effective concentration in the visible region was ∼10 μM.

Time-resolved difference spectra (373−521 nm) were collected at 50 delay times between 50 ns and 50 ms after photolysis of the fully reduced CO complex. Calculation of the resultant difference spectra (transient absorption minus the prephotolysis ground state) included a correction for the "dark counts" of the detector and a base-line correction. Data arrays containing difference spectra at 44 delay times (50 ns to 9.2 ms) were analyzed using singular value decomposition (SVD) as previously described (*11*, *27*, *28*). The results of the analysis, the **u**-spectra and **v**-vectors, and a semilogarithmic plot of the singular values were used to estimate the number of processes present. Reduced **U** and **V** matrices, composed of the first few (usually 10) **u**-spectra and **v**-vectors resulting from the SVD, were used in further analysis. The **V** matrix was subjected to global exponential fitting to determine the apparent lifetimes, and the optimized parameters were used to calculate the associated spectral changes (**b**-spectra) of the processes involved. The data matrices were also analyzed using a double difference map representing changes in absorbance of the reaction mixture as a function of delay time and wavelength. On the basis of this analysis and an analogous one of spectra recorded in the visible region, a kinetic mechanism was proposed from which the difference spectra of the intermediates were determined. We chose to represent such spectra as referenced against the oxidized enzyme. The validity of the mechanism was tested by comparing the extracted difference spectra (experimental difference spectra) to model difference spectra. The latter were linear combinations of ground-state spectra of the oxidized, reduced, mixed-valence CO and fully reduced CO complexes, the reduced-minus-oxidized spectrum of Cu_A from *Thermus thermophilus* (*29*) and the spectra of the 607 and 580 nm (ferryl) derivatives. The 607 nm species with maxima at 606 and 437 nm and a trough at 414 nm, and the 580 nm form with peaks at 580 and 434 nm and a trough at 413 nm (referenced against the oxidized enzyme) were prepared as previously described (*30*). The yields of the ferryl and the 607 nm species were 50−60% on the basis of their difference spectra using extinction coefficients of 11 mM^{-1} cm^{-1} at 607−630 nm and 5.3 mM^{-1} cm^{-1} at 580−630 nm for the 607 and 580 nm species, respectively (*12*). The spectra were normalized using these extinction coefficients to obtain the effective concentration in the photolysis experiments (the concentration after photolysis). The spectra of the two species corresponded well to previously published spectra (*12*, *30*), indicating that these were of pure P and F and not a mixture of the two.

RESULTS

The Soret time-resolved difference spectra (post- minus prephotolysis) are shown in Figure 1. Analogous difference spectra in the visible region have been published previously (*11*). The spectra represent 44 delay times (expanding exponentially) between 50 ns and 9.2 ms. The difference spectrum at 50 ns has a peak at 446 nm and a trough at 415 nm and is identical to the one obtained in the absence of O_2 under otherwise identical experimental conditions.

Singular Value Decomposition and Double Difference Map. The **u**-spectra (orthonormal basis spectra) and the **v**-vectors, which represent the time evolution of the corresponding **u**-spectra, are obtained from SVD analysis of the transient difference spectra. As pointed out in our previous paper (*11*), each **u**−**v** pair reflects spectral and temporal changes of several processes. In the visible region, a relatively good separation of individual processes was observed in the **u**-spectra and **v**-vectors (*11*). It is more difficult to assign **u**−**v** couples to individual processes in the Soret region due to overlapping absorbances of the intermediates, but qualitative information can be obtained from a two-dimensional map of the double difference spectra ($\Delta\Delta\mathbf{A}$). The double difference map represents a top view of a three-dimensional plot of the time-resolved $\Delta\Delta\mathbf{A}$ as a function of time and wavelength, where the dark and light

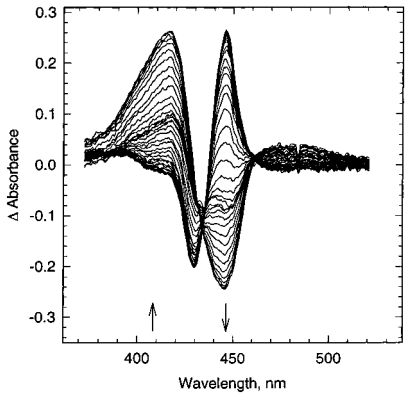

FIGURE 1: Time-resolved absorption difference spectra (post- minus prephotolysis) collected during the reaction of the fully reduced cytochrome oxidase with dioxygen. The spectra represent 44 delay times, equally spaced on a logarithmic scale, between 50 ns and 9.2 ms after photolysis of the fully reduced CO complex. Each spectrum represents the average of 19 accumulations. The arrows indicate the direction of the spectral changes with time. The effective cytochrome oxidase concentration (concentration after photolysis) was 3.6 μM in 0.1 M sodium phosphate buffer (pH = 7.4) at 25 °C. The CO and O_2 concentrations after mixing were 0.05 atm (~0.05 mM) and 625 μM, respectively.

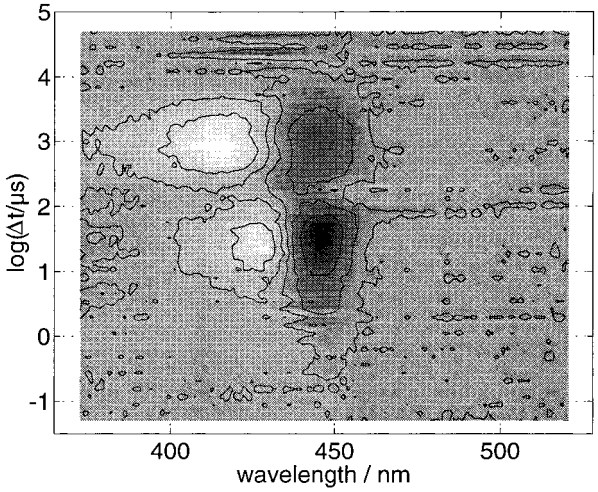

FIGURE 2: Smoothed double difference map (the top view of a three-dimensional plot representing the time-resolved double difference spectra, $\Delta\Delta\mathbf{A}$) as a function of log(delay time) and wavelength. The double difference spectra were obtained by subtracting each time-resolved difference spectrum from the preceding spectrum (see text for details). The rates of absorbance decrease and increase are indicated by darker and lighter shadings, respectively.

shadings indicate the normalized rate[2] of absorbance decrease and increase, respectively.

The double difference map in the Soret region shows an absorbance decrease at 445 nm on the 200 ns to 1 μs time scale (Figure 2). These absorbance changes are followed by a drop in absorbance at 445 nm between 1 and 10 μs. Between 20 and 70 μs, there is a sharp absorbance decrease at ~445 nm that occurs on the same time scale as a profound decrease in absorbance at 605 nm in the double difference

[2] The exponentially increasing spacing between consecutive delay times results in the differences between subsequent pairs of spectra being effectively multiplied by the difference in delay times. This offers a beneficial scaling (normalization) of $\Delta\Delta\mathbf{A}$. If $\Delta\Delta\mathbf{A}$ were calculated as the true rate of absorbance change, the fastest rates would dominate the map topography.

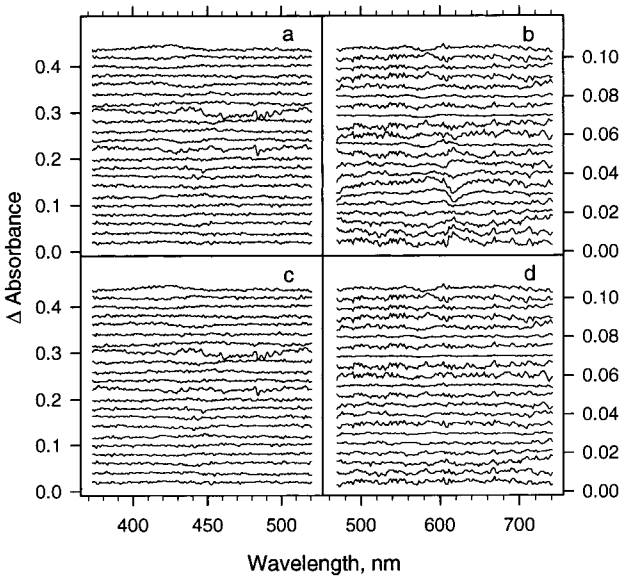

FIGURE 3: Residuals (data minus the least-squares fit) from a four-exponential fit (a and b) and five-exponential fit (c and d) of the time-resolved Soret data in Figure 1 (panels a and c) and the baseline-corrected time-resolved visible data in ref 11 (b and d). Every other time point is plotted and the delay times decrease from top to bottom. The residuals are separated by a constant factor for clarity.

visible map (*11*). Simultaneously, there is an increase in the absorbance at ~430 nm. These spectral changes most probably reflect the conversion of the ferrous−oxy complex (compound A) to the subsequent intermediate, including the oxidation of cytochrome *a* which has an absorbance maximum at ~426 nm (*31*). Between 100 and 130 μs an increase in absorbance at 445 nm is simultaneous with an absorbance increase at 605 nm in the double difference visible map, which was attributed to the reduction of cytochrome *a* (*11*). These spectral changes are followed by a second decrease in absorbance at 445 nm at ~1 ms and an increase in the rate of absorbance at ~415 nm, which correspond to the reoxidation of cytochrome *a* and the conversion of cytochrome a_3 to its oxidized state.

Multiexponential Fitting by Nonlinear Regression. The truncated **V** matrices from the SVD were analyzed using global exponential fitting with an increasing number of exponentials. After including each additional exponential, the residuals, i.e., differences between the fit and the data, were compared. There was a clear improvement upon increasing the number of exponentials from three to four. The residuals from a four-exponential fit of the data in Figure 1 and of the previously published visible data (*11*) with baseline correction are shown in Figure 3, panels a and b, respectively (every other time point is plotted). The apparent lifetimes (τ = 1/(rate constant)) for the Soret region were 0.8 μs, 36 μs, 97 μs, and 1.2 ms and for the visible region 10 μs, 43 μs, 75 μs, and 1.4 ms. The Soret lifetimes (with associated errors) represent a unique fit in that region; i.e., these lifetimes represent a local minimum and were the convergence result regardless of the initial starting values. In the visible region, a nonrandom pattern was apparent in the residuals on early microsecond time scale (Figure 3b) so that another lifetime was necessary to satisfactorily fit the data. When the visible data were analyzed with five rather than four exponentials (Figure 3d), the nonrandom pattern

in the residuals resulting from the four-exponential fit disappeared. The respective five lifetimes were 1.0 ± 0.4 μs, 15 ± 5 μs, 36 ± 5 μs, 90 ± 25 μs, and 1.4 ± 0.1 ms, which represents a unique fit under the same tolerance conditions. The error intervals were estimated from experiment-to-experiment variation rather than from error analysis of each data set. Therefore at least five exponentials are required to fit the visible data, a conclusion supported by results from numerous experiments which were consistently fitted with five apparent lifetimes within the errors reported above. Similar lifetimes, except the 1 μs lifetime, have been reported previously (*32*−*34*).

In the Soret region the difference in quality of the fit between four and five exponentials is not clear (Figure 3a,c). This is primarily due to spectral overlap between intermediates in the Soret region but also due to more frequent occurrence of artifacts (structured, not noiselike departures from zero) in the residuals in the Soret region compared to those in the visible region. Thus, the visible region is a better diagnostic tool for the number of processes present than the Soret region. In the Soret region there is more than one set of five lifetimes; i.e., there is not a local minimum that dominates and leads to a unique set of five lifetimes. However, under the restriction that any two lifetimes must be at least a factor of 2 apart, all five exponential fits in the Soret region fall within the range of values obtained for the visible region. In the absence of this restriction, successive lifetimes tend to merge, resulting in **b**-spectra that cannot be interpreted. The standard error of the fits for all the Soret sets falls within a narrow range (1−2%) and is lower than the error for the four-exponential fit. On the basis of these results and the reproducibility of the five exponentials in the visible region, we therefore fitted to the Soret data a model comprising five apparent lifetimes, 0.9 ± 0.5 μs, 8.3 ± 4.0 μs, 36 ± 10 μs, 103 ± 30 μs, and 1.2 ± 0.1 ms. These are in accordance with our previously published values for the visible region (*11*), excluding the 25 μs process. Our earlier report used data only from the visible region, and a sixth 25 μs lifetime was included on the basis of information contained in the visible double difference map.

Although the residuals between the four- and five-exponential fits are not noticeably improved in the Soret region (Figure 3a,c), the fits to the first few **v**-vectors are improved, further justifying the use of the five-lifetime model for both spectral ranges. Figure 4 shows the difference between the Soret region's first three **v**-vectors and a four-exponential fit (panel a) and a five-exponential fit (panel c). A difference between analogous **v**-vectors and four- and five-exponential fits is shown for the visible region in Figure 4b,d, respectively. The fit to the **v**-vectors is significantly improved in both regions upon going from four- to the five-exponential fit.

A semilogarithmic plot of the Soret region's first singular values [15.42, 1.70, 0.33, 0.20, 0.16, 0.096, 0.056, 0.047, 0.042, 0.038, ...] provides an estimate of the number of intermediates present. The plot (not shown) supports the conclusion that at least six intermediates (five processes) are present since the first six singular values are clearly above the noise. The Soret spectral changes (**b**-spectra) resulting from the five-exponential fit of the transient difference spectra referenced against the oxidized enzyme are shown in Figure 5.

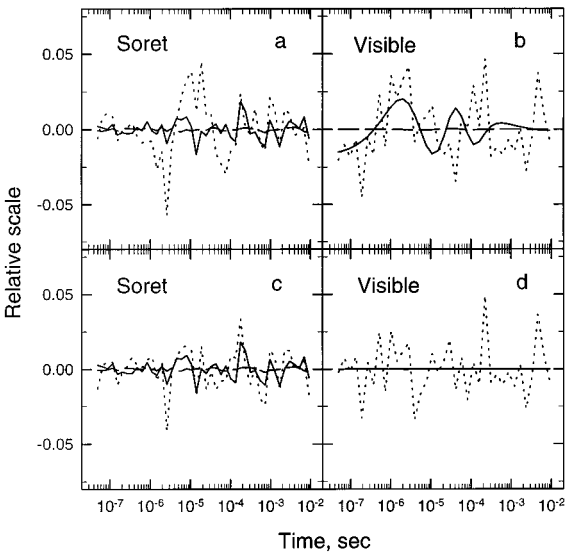

FIGURE 4: Difference between the first three **v**-vectors resulting from the SVD analysis and a four-exponential fit (a and b) and a five-exponential fit (c and d) of the time-resolved Soret data (a and c) and the base-line-corrected time-resolved visible data in ref 11 (b and d). The reference for both sets of data was the oxidized enzyme. The solid, dotted, and dashed lines represent the difference between the first, second, and third **v**-vectors, respectively, and the fits.

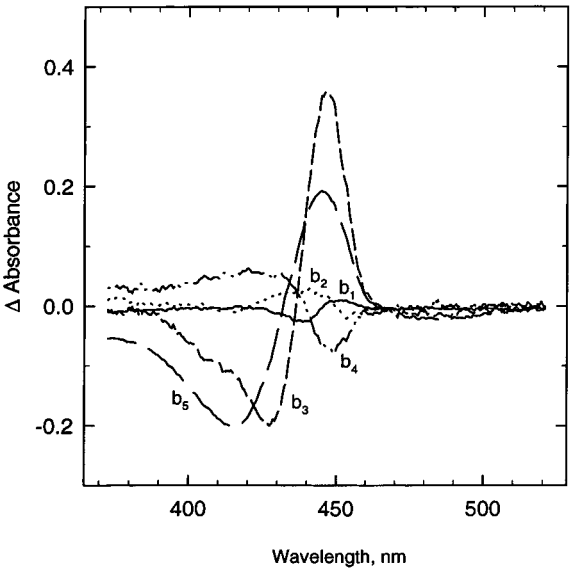

FIGURE 5: Spectral changes (**b**-spectra) from the five-exponential fit of the time-resolved Soret data referenced versus the oxidized enzyme. The apparent lifetimes were 0.9 μs for $\mathbf{b_1}$, 8.3 μs for $\mathbf{b_2}$, 36 μs for $\mathbf{b_3}$, 103 μs for $\mathbf{b_4}$, and 1.2 ms for $\mathbf{b_5}$.

DISCUSSION

Kinetic Mechanism and Spectra of Intermediates. The global exponential fitting analysis gives information about the minimum number of processes present, the **b**-spectra and apparent lifetimes. The next step involves testing different mechanisms and extracting the spectra of the intermediates. The kinetic mechanism in Scheme 1 is based on observations from the SVD, the double difference maps, and global exponential fitting of data both in the visible and Soret regions. The model builds on our earlier model based on data only from the visible region (*11*) but provides a more complete mechanism that fits results from both spectral regions.

Scheme 1: Proposed Mechanism for the Reduction of Dioxygen to Water by Cytochrome *c* Oxidase[a]

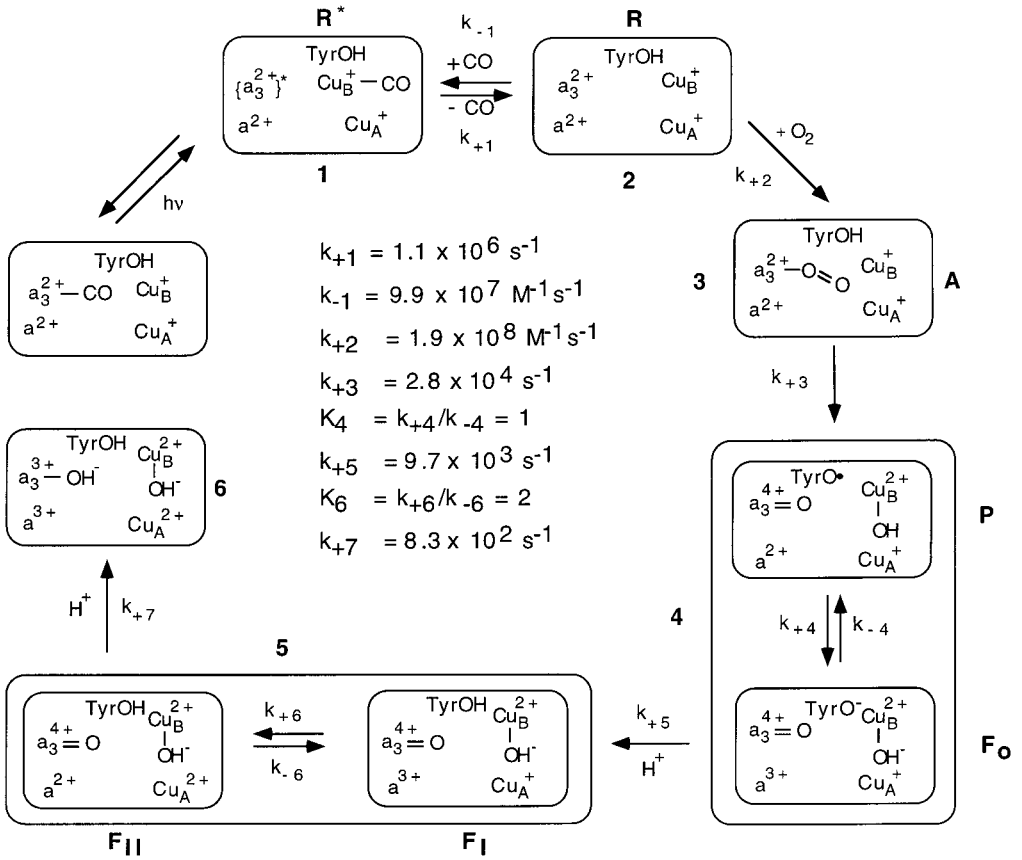

[a] The pure spectra of P and F_o are not resolved experimentally, but intermediate 4 represents a 1:1 mixture of the two. The same is true for F_I and F_{II}, but the ratio of the two is 1:2. Tyrosine 244, represented here as TyrOH, is postulated to function as an H-atom donor during the cleavage of the O−O bond (A → P).

The main criteria for the validity of a particular mechanism were good agreement between experimental and theoretical lifetimes and between the experimental and model spectra of the intermediates depicted in Scheme 1. Reverse rate constants were not included in the model (except for the first step in which both the forward and the reverse rate constants are firmly established (*35*)) unless required to get a good fit between the experimental and model difference spectra. The model difference spectra of the intermediates in Scheme 1 were obtained from linear combinations of ground-state spectra of known derivatives of the enzyme. In addition to the spectra of the oxidized, reduced, mixed-valence CO and fully reduced CO species, and 607 and 580 nm (ferryl) derivatives, the reduced-minus-oxidized difference spectrum of Cu_A from *Thermus thermophilus* was used (*29*). The reduced-minus-oxidized difference spectrum of cytochrome *a*, without interference from Cu_A, was obtained by subtracting the spectrum of the mixed-valence CO complex and the reduced-minus-oxidized spectrum of Cu_A from the spectrum of the fully reduced CO enzyme. The reduced-minus-oxidized spectrum of cytochrome a_3 (and Cu_B) was obtained by subtracting the reduced-minus-oxidized difference spectra of cytochrome *a* and Cu_A from the reduced-minus-oxidized difference spectrum of the enzyme. All the difference spectra are referenced against the oxidized enzyme unless otherwise noted and all represent 100% of the respective intermediate.

Intermediates 1 and 2 (R and R).* In accordance with our previous model (*11*), the first step in Scheme 1 involves the relaxation of cytochrome a_3 to the fully reduced form. Cytochrome a_3 has been suggested to have different conformations in R* and R, possibly related to CO binding to Cu_B^+ (*35*). The experimental spectrum of intermediate 1 (R*) (not shown) is similar to that of intermediate 2 (R) but slightly red-shifted, in agreement with our previous results obtained in the absence of O_2 (*27*). There is excellent agreement between the experimental and model difference spectra (referenced versus the oxidized enzyme) of the unliganded reduced intermediate, R (Figure 6).

Compound A. The formation of the fully reduced enzyme, R, is followed by the binding of O_2 to cytochrome a_3, forming compound A (Scheme 1). The difference between compound A and the reduced enzyme ($a_3^{2+}-O_2$ minus a_3^{2+}) (Figure 7, solid line) reflects spectral changes due to O_2 binding to cytochrome a_3 and without the interference from cytochrome *a*. The difference spectra were modeled by the spectrum of the fully reduced CO complex referenced against the fully reduced enzyme (Figure 7, dotted line), which accounts for the apparent discrepancy between the model and experimental spectra. The Soret difference spectrum of compound A is shifted ~8 nm to the blue in the Soret region compared to the CO-bound complex, which has a maximum at 430 nm, and its intensity is also significantly smaller than that of the corresponding CO-difference spectrum, in agreement with model studies of Babcock and Chang (*36*).

The pseudo-first-order microscopic rate constant for the formation of the ferrous−oxy complex, $k_2' = k_2[625 \times 10^{-6}\ \text{M}\ O_2] = 1.2 \times 10^5\ s^{-1}$ ($\tau = 8.3\ \mu s$) is ~5 times larger than k_3 in Scheme 1, while, in our previously published scheme

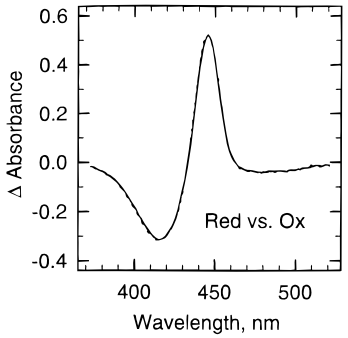

FIGURE 6: Comparison of the experimental (solid line) and model (dotted line) difference spectra of intermediate 2 (R) present during the reaction of the fully reduced enzyme with dioxygen (the spectrum of the oxidized enzyme was used as a reference). The experimental spectrum was determined on the basis of the mechanism and the microscopic rate constants in Scheme 1. The model spectrum is the spectrum of the fully reduced form of the enzyme referenced against the oxidized form.

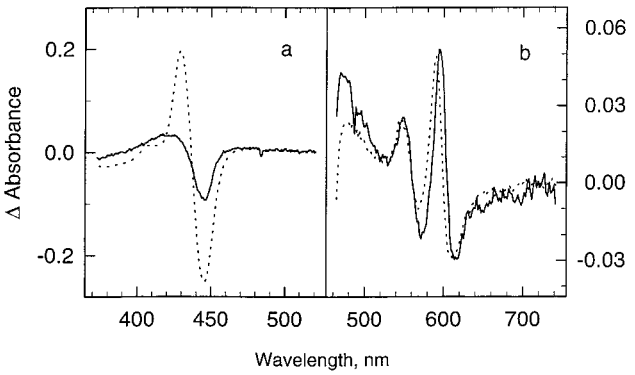

FIGURE 7: (Solid line) Difference between the experimental spectrum of intermediate 3 (compound A) and the experimental spectrum of intermediate 2, $a_3^{2+}-O_2$ minus a_3^{2+} (Scheme 1) in (a) the Soret region and (b) the visible region. The model spectrum (dotted line) is the difference between the spectrum of the fully reduced CO complex and the fully reduced unliganded enzyme, $a_3^{2+}-CO$ minus a_3^{2+}. The effective concentration of cytochrome oxidase was 3.6 and 10 μM in the Soret and visible regions, respectively.

based solely on data in the visible region, k_3 was 1.5 times faster than k_2' (*11*). The visible difference spectrum between compound A and the fully reduced unliganded enzyme ($a_3^{2+}-O_2$ minus a_3^{2+}) using the five-exponential model and the corresponding lifetimes reported above, is shown in Figure 7b (solid line). The spectrum is similar to our previously published spectrum (*11*), except the intensity is lower, or on par, with the fully reduced CO-bound enzyme.

Intermediate 4. The experimental difference spectrum of intermediate 4 in the Soret region is shown in Figure 8a (solid line). The Soret difference spectrum of the 607 nm species (referenced versus the oxidized enzyme), obtained upon exposure of an oxidized enzyme solution to a mixture of CO and O_2, is shown as the dotted line in Figure 8a. The dashed line represents the same 607 nm cytochrome a_3 species, but cytochrome *a* is 15% reduced and 85% oxidized as suggested by the visible data (*11*). Figure 8b shows analogous spectra in the visible region. It is clear that the experimental spectrum of intermediate 4 does not match that of either model spectra, with the Soret experimental difference spectrum having significantly larger intensity in both the peak and the trough. On the basis of our previous studies

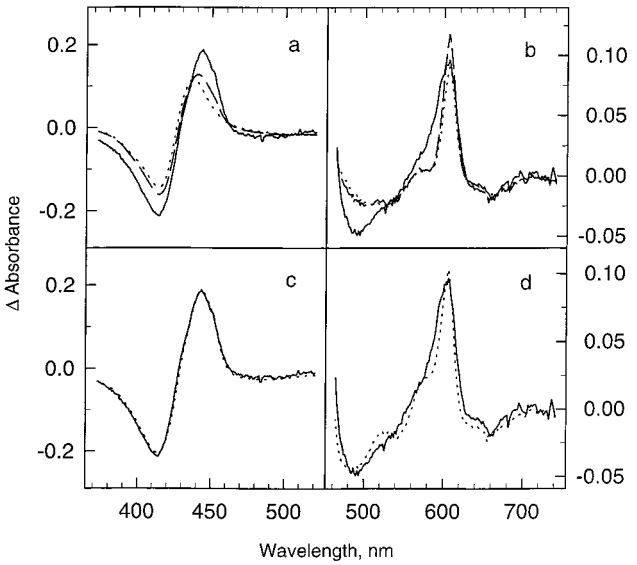

FIGURE 8: The experimental (solid lines) and model (dotted and dashed lines) difference spectra of intermediate 4 in the Soret region (a and c) and visible region (b and d). The reference spectrum is that of the oxidized enzyme. (a and b) The dotted and dashed lines represent the model spectra of the 607 nm species alone and after the addition of 15% of the reduced-minus-oxidized spectrum of cytochrome *a*, respectively. (c) The model spectrum for the Soret region (dotted line) is made up of 50% 607 nm species, 50% 580 nm form, 50% reduced-minus-oxidized cytochrome *a*, and 100% reduced-minus-oxidized Cu_A. (d) The model spectrum for the visible region (dotted line) is made up of 40% 607 nm species, 60% 580 nm form, 40% reduced-minus-oxidized cytochrome *a*, and 100% reduced-minus-oxidized Cu_A (see text for more details).

in the visible region, we suggested that the structure of cytochrome a_3 in intermediate 4 was identical to the species produced upon exposing a solution of the oxidized enzyme to CO in the presence of O_2 (*11*), since both the experimental and model difference spectra of intermediate 4 showed a peak with the same intensity at 606 nm (Figure 5d in ref *11*). However, a discrepancy in the bandwidth between the two was noted.

The difference in intensity between the experimental and model Soret spectra (Figure 8a) and the previously noted discrepancy in bandwidth between the two in the visible region (*11*) (Figure 8b) suggests that the structure of cytochrome a_3 in intermediate 4 is not equivalent to the model 607 nm species. In fact, the experimental difference spectra of intermediate 4 in the Soret *and* visible regions can be best modeled by assuming that the intermediate is made up of approximately a 1:1 mixture of the 607 and 580 nm (ferryl) species, with cytochrome *a* reduced in the former but oxidized in the ferryl. We propose that compound A decays with an apparent lifetime of 36 μs to the 607 nm species (P), which subsequently is rapidly converted to F_o (Scheme 1). The rate constants for the intercoversion between the 607 nm species and F_o must be significantly faster than the 36 μs lifetime since the spectrum of the pure 607 nm species cannot be resolved. In Figure 8c, the Soret experimental difference spectrum of intermediate 4 (solid line) is modeled (dotted line) using 50% of the 607 nm species, 50% of the 580 nm ferryl (F_o), 50% of the reduced-minus-oxidized cytochrome *a*, and 100% of the reduced minus-oxidized Cu_A. Analogous spectra are shown for the visible region in Figure 8d, except that 40% of the 607 nm species, 60% of the 580 nm ferryl, 40% of the reduced-minus-oxidized cytochrome

a, and 100% of the reduced minus-oxidized Cu_A were used to construct the model difference spectrum. In Scheme 1, the 607 nm species is proposed to be a_3^{4+}═O Cu_B^{2+}−OH^-, with a radical on tyrosine 244. This tyrosine has recently been shown to be covalently bound to the histidine 240 ligand of Cu_B in the bovine enzyme (*37*), and an analogous cross-link has been reported for the enzyme from *Paracoccus denitrificans* (*38*). Upon conversion of the 607 nm species to F_o, cytochrome *a* donates an electron to the tyrosine radical producing tyrosinate.

As noted above, our previous interpretation of the visible spectra alone produced a mechanism in which intermediate 4 was proposed to be the 607 nm species with 15% of cytochrome *a* reduced. It is coincidental that our early model and the new model match the intensity of the experimental spectrum of intermediate 4 at 606 nm. The lower proportion of the 607 nm intermediate (and therefore lower intensity at 606 nm) in the new model is compensated by a higher proportion of reduced cytochrome *a* (50% versus 15% in the older model) which has maximum absorbance at ∼605 nm, similar to the maximum of the 607 nm species. The discrepancy in bandwidth between the experimental and model spectra appears to be less in the new model (Figure 8b,d). It is also clear that our previous model does not fit well in the Soret region (Figure 8a) but that a ∼1:1 mixture of the 580 nm species and the 607 nm species with cytochrome *a* reduced provides a reasonable fit to intermediate 4 in both regions (Figure 8c,d).

It should be emphasized that the mechanism in Scheme 1 is based on the assumption that the spectra of the intermediates in the dioxygen reduction reaction are equivalent to spectra of known derivatives of the enzyme, including those of the 607 nm species and the 580 nm form. Thus our analysis compares experimental and model spectra of known derivatives of the enzyme having hemes and coppers in fixed redox and/or ligation states and does not take into account possible heme−heme or heme−copper spectral interactions. For example, the model spectrum of the 607 nm species in Scheme 1 is produced by adding the reduced-minus-oxidized spectra of cytochrome *a* and Cu_A to the spectrum of the 607 nm species. The latter is generated by adding CO/O_2 to the oxidized enzyme, and both cytochrome *a* and Cu_A are oxidized. However, in the 607 nm species postulated in Scheme 1, both cytochrome *a* and Cu_A are reduced. It is possible that the spectrum of the 607 nm species is affected by the redox states of cytochrome *a* and Cu_A, and such spectral interactions could account for the difference between the experimental and model spectra of intermediate 4 in the visible region (Figure 8d). In the case of strong spectral interactions, we cannot exclude the possibility that intermediate 4 represents a pure 607 nm species with cytochrome *a* and Cu_A reduced, but with a spectrum significantly different from that obtained upon adding the reduced-minus-oxidized spectra of cytochrome *a* and Cu_A to the spectrum of the model 607 nm species made with cytochrome *a* and Cu_A oxidized. Experiments on the reaction of the mixed-valence enzyme with dioxygen could help resolve this issue.

It should also be noted that the Cu_A spectrum was recorded in a different organism (*Thermus thermophilus*) (*29*). However, it appears to be qualitatively similar to that of the bovine enzyme on the basis of the good correspondence between the experimental and model spectra in the Cu_A spectral region (480−550 nm) (Figure 8d, Figure 9b,d).

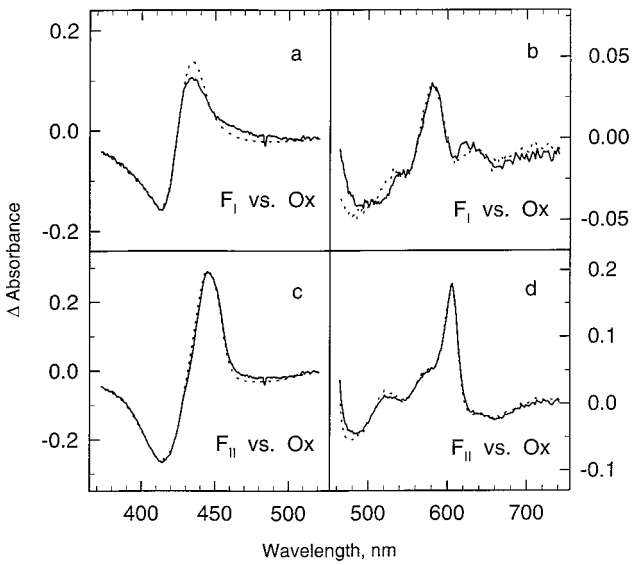

FIGURE 9: (a) Experimental (solid lines) and model (dotted lines) difference spectra of F_I (a and b) and F_{II} (c and d) referenced against the oxidized enzyme. The oxidation states of the heme and copper centers in the difference spectrum of F_I are a_3^{4+}═O−a_3^{3+}, Cu_A^{+}−Cu_A^{2+} and in F_{II} a_3^{4+}═O−a_3^{3+}, a^{2+}−a^{3+}.

F_I and F_{II}. In Scheme 1, a proton is postulated to be taken up by tyrosinate on a 100 μs time scale (see below), resulting in the formation of F_I; this is followed by faster electron transfer between Cu_A and cytochrome *a*, resulting in F_{II}, a_3^{4+}═O Cu_B^{2+}−OH a^{2+} Cu_A^{2+}. The rate constants for the intercoversion between F_I and F_{II} must be significantly faster than the 100 μs lifetime since the spectrum of pure F_I is not easily resolved. Although the rate constants for the inverconversion between F_I and F_{II} are unknown, the equilibrium constant, $K_6 = k_{+6}/k_{-6}$, must be close to 2 since a mixture of model spectra of F_I and F_{II} in a ratio of 1:2 best fits the experimental spectrum of intermediate 5. The experimental difference spectrum of F_I, shown in Figure 9a (solid line), was obtained by subtracting the 67% contribution of the reduced-minus-oxidized cytochrome *a* spectrum and the 67% of the oxidized-minus-reduced Cu_A spectrum from the experimental difference spectrum of intermediate 5. Correspondingly, upon adding 33% of the reduced-minus-oxidized spectrum of cytochrome *a* and 33% of the oxidized-minus reduced spectrum of Cu_A to the experimental difference spectrum of intermediate 5, the experimental difference spectrum of F_{II} was obtained (Figure 9c, solid line). The experimental visible difference spectra of F_I and F_{II} using a five-exponential fit (apparent lifetimes of 1 μs, 15 μs, 36 μs, 90 μs, and 1.4 ms) are shown in Figure 9b and 9d (solid lines), respectively.

The model Soret and visible difference spectra of F_I, referenced versus the oxidized enzyme (Figure 9a,b, dotted lines), were obtained by adding the reduced-minus-oxidized difference spectrum of Cu_A to the difference spectrum of the species produced upon addition of excess hydrogen peroxide to an oxidized enzyme solution. The model difference spectra of F_{II} as depicted in Scheme 1 (Figure 9c,d, dotted lines) were obtained by adding the reduced-minus-oxidized spectrum of cytochrome *a* and the oxidized-minus-reduced spectrum of Cu_A to the model difference spectra of F_I. In both the Soret and visible regions, there is an excellent

correspondence between the model and experimental difference spectra of F_I and F_{II}. For F_I, both the model and experimental difference spectra have a peak at 580 nm in the visible region (Figure 9b), and in the Soret region both difference spectra have a maximum at 434 nm and a minimum at 413 nm (Figure 9a). The identical redox states of Cu_A in the experimental and model difference spectra have practically eliminated the previously observed discrepancy in the 480−550 nm region between the two spectra (*11*), which incidentally was suggested to result from the different oxidation states of Cu_A in the model and experimental difference spectra.

The structure of the ferryl species in intermediate 4 (F_o) and intermediate 5 (F_I and F_{II}) is postulated to be a_3^{4+}=O with respect to cytochrome a_3, since for both intermediates the spectrum of the 580 nm species can be used as the model spectrum. However, in F_o tyrosine is deprotonated while protonated in F_I/F_{II} (Scheme 1), which could account for some spectral differences between the two. This difference could be the source of discrepancy between the experimental and model difference spectra of intermediate 4 in the visible region (Figure 8d). Hallén and co-workers (*34*, *39*) and studies in our laboratory[3] have shown that a proton is indeed taken up on ∼100 μs time scale, that is during the conversion of intermediate 4 to intermediate 5. It appears likely that a proton is taken up by the tyrosinate rather than by Cu_B^{2+} considering the higher pK_a of the former. Hydrogen bonding could also be different in F_o and F_I/F_{II}, causing spectral differences between the two (*40*). An alternative explanation for a difference between the ferryls in intermediates 4 and 5 is that a conformational change occurs upon conversion of intermediate 4 to intermediate 5.

In our previous model of the O_2 reduction by cytochrome oxidase based on data only from the visible region, we added an additional lifetime for the electron transfer between cytochrome *a* and Cu_A, which allowed separation of the F_I and F_{II} species. The additional lifetime was based on information from the double difference visible map and not on the global analysis (*11*). As discussed above, the Soret region did not warrant a sixth lifetime and therefore F_I and F_{II} are observed as a mixture. The electron-transfer rate between Cu_A and cytochrome *a* has previously been measured for two states of the enzyme. Using photochemically activated compounds, an apparent lifetime of 50−60 μs was obtained for the state of the enzyme in which the oxygen binding site was oxidized (*41*−*43*). Photolysis experiments on the mixed-valence and three-electron-reduced CO complexes gave similar lifetimes (∼50 μs) for the electron transfer between cytochrome *a* and Cu_A (*27*, *28*, *44*−*46*). Interestingly, we did not observe the 50 μs process, and the rate of electron transfer between cytochrome *a* and Cu_A appears to be significantly faster than the decay rate of intermediate 4 (∼90−100 μs) since it does not easily emerge from the global fitting. This indicates that the proton uptake on ∼100 μs time scale is rate-limiting electron transfer between Cu_A and cytochrome *a* (*34*, *47*). Therefore it is possible that the electron-transfer rate is faster under the conditions when the oxygen binding site is in the ferryl state. In our previous work, an apparent lifetime of ∼30 μs was postulated (k_{+5} and k_{-5}; ref *11*) for the electron transfer between cytochrome *a* and Cu_A, but more recent analysis suggests that this rate could be even faster.[3] On the basis of the coupling efficiencies of the 14 covalent bonds present on the electron-transfer pathway between Cu_A and cytochrome *a*, Gray and co-workers estimated a lifetime of 1.2−25 μs for electron transfer between the two redox centers, the range depending on the reorganization energy (0.15−0.5 eV) (*48*).

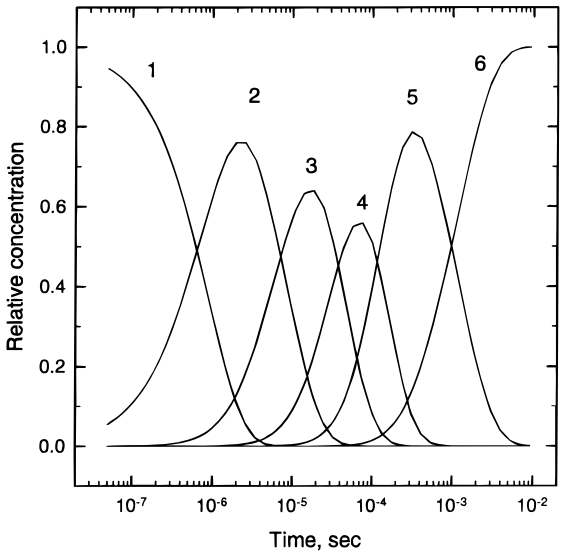

FIGURE 10: Time-dependence of the concentration profiles for the intermediates present during the reaction of the fully reduced enzyme with dioxygen. The profiles are based on the mechanism and microscopic rate constants in Scheme 1.

Time−*Concentration Profiles.* Figure 10 shows the concentrations of the various intermediates as a function of time based on the mechanism and rate constants in Scheme 1. The profiles are similar to those previously published in the visible region (*11*) in terms of the time scales at which the intermediates reach their maximum concentrations. The Soret data presented here were fitted with five lifetimes rather than six, and the time−concentration profiles of F_I and F_{II} are represented by one curve rather than two. For either scheme, F_I and F_{II} together reach a maximum concentration ∼330 μs after photolysis. One difference between these profiles and those based on the six-exponential fit (*11*) is the relative amplitude of intermediate 3 (compound A) and intermediate 4. In Scheme 1 (five-exponential fit), k_3 (2.8×10^4 s^{-1} = 1/36 μs^{-1}) is smaller than the pseudo-first-order rate constant for O_2 binding in Scheme 1, k_2' (1.2×10^5 s^{-1} = 1/8.3 μs^{-1}), and the maximum concentration of compound A at ∼30 μs is larger than that of the following species, intermediate 4. In the six-exponential model (*11*), k_3 was ∼1.5 times larger than the pseudo-first-order rate constant for O_2 binding, and consequently the maximum concentration of intermediate 3 was significantly less than that of intermediate 4. Since the revised five-exponential model (Scheme 1) gives good correspondence between the experimental and model spectra when *both* the Soret and visible regions are analyzed, we favor the order of rate constants in Scheme 1 over that previously proposed. The overlap between the time windows of intermediate 4, compound A, and intermediate 5 might explain why intermediate 4 has been difficult to detect by time-resolved resonance Raman (TR[3]) (*24*).

Bose et al. (*25*) recently studied single-turnover kinetics of cytochrome oxidase reduction of O_2 and reported four

[3] Unpublished results.

lifetimes of 0.01, 0.1, 1.1, and 30 ms on the basis of singular value decomposition. The first three lifetimes are the same as those reported here, while the 1 μs lifetime observed in our studies was not detected within their time resolution. The 30 ms lifetime might represent the conversion of intermediate 6 in Scheme 1 to the final oxidized enzyme. The 36 μs lifetime, clearly observed in our analysis of the visible spectra, was not observed in the study of Bose et al. (*25*). A possible reason for this is that the experiments of Bose et al. were carried out at 5 times lower final oxygen concentration compared to our experiments (125 μM versus 625 μM in our case). At 125 μM oxygen, O_2 binding becomes rate-limiting, which precludes the simultaneous observation of both the 10 and 36 μs lifetimes. Another possible reason for not observing both the 10 and 36 μs lifetimes is the fact that experiments of Bose et al. (*25*) were carried out simultaneously in the visible and the Soret regions at a maximum of 5 μM cytochrome aa_3, at which concentration the Soret region has a substantial intensity while the visible region does not. In this case one would expect the Soret region to become the determining factor in establishing how many lifetimes are present. However, as discussed above, a clear distinction between four and five lifetimes, the latter including both the 10 and the 36 μs lifetimes, cannot be made if only the data in the Soret region are used. For instance, if we only considered the Soret data in our analysis, the 36 μs lifetime and not the 10 μs lifetime is observed. In our experiments, the visible data were recorded at an effective oxidase concentration (concentration after photolysis) of 10−20 μM which allowed high signal-to-noise ratio in this region and the resolution of five lifetimes.

Structure of Intermediate 4. Time-resolved and steady-state resonance Raman studies by Ogura and co-workers have suggested that the O−O bond is broken in the 607 nm species as well as in the ferryl species represented by intermediate 5 (F_I and F_{II}), and the resonance lines at 804 and 785 cm^{-1} have been assigned to the 607 nm species and the 580 nm ferryl form, respectively (*21*, *49*−*51*). These investigators have suggested that the structure of the binuclear center in the 607 nm species is a_3^{5+}═O Cu_B^{2+}. Species in which cytochrome a_3 is in a ferryl state, a_3^{4+}═O, with an oxidizing equivalent on Cu_B (Cu_B^{3+}) or in which an amino acid provides the extra oxidizing equivalent, have also been proposed (*20*, *30*). On the basis of magnetic circular dichroism studies, Palmer and co-workers have provided arguments against the 607 nm species being a_3^{4+}═O Cu_B^{2+} with a porphyrin radical (*16*).

In our modeling of intermediate 4, the best fit is obtained if one assumes a 1:1 mixture of the 607 nm species and the 580 nm ferryl form, with cytochrome *a* reduced in the former and oxidized in the ferryl. As noted above, if the decay of compound A to the 607 nm species occurs with an apparent lifetime of 36 μs, a 1:1 mixture of the 607 and 580 nm forms could be accomplished by a rapid interconversion between the two species with an equilibrium constant of 1 (Scheme 1). In this case, we would not know the rate constants for the interconversion, but they would be rapid enough to preclude the observation of the 607 nm species as a pure intermediate. However, if cytochrome a_3 in the 607 nm species is in a state in which the O−O bond has not been cleaved, i.e., in a true peroxy state (a_3^{3+}−O^-−O^- or a_3^{3+}−O^-−OH), this would require that O−O bond cleavage chemistry be reversible, which has not been demonstrated experimentally.

Alternatively, if one assumes a rapid interconversion between the 607 nm species and the ferryl of intermediate 4, and if the 607 nm species is a ferryl, rather than a peroxy species, the most likely structure for the binuclear center in the 607 nm species would be a_3^{4+}═O Cu_B^{2+}−OH^- with an associated amino acid radical (Scheme 1). A plausible candidate for such a radical would be tyrosine 244 (tyrosine 280 in the *Paracoccus* enzyme) which has recently been shown by crystallographic studies to be cross-linked to one of the histidine ligands (His240) of Cu_B (*37*, *38*). Furthermore, steady-state resonance Raman data of Ogura and co-workers have shown that the 607 nm species corresponds to the 804 cm^{-1} mode, which has been unequivocally assigned to a ferryl (*21*, *49*−*51*). Taking into account these data and the results presented here, we propose that the O−O bond is cleaved upon formation of the 607 nm intermediate and that tyrosine 244 donates a hydrogen atom during the O−O bond cleavage. Recent studies of Babcock and co-workers on the reaction of the mixed-valence enzyme with dioxygen support this conclusion (*40*). In this case, the difference between the spectra of P (607 nm species) and F (580 nm form) arises from interactions of the radical with the electronic structure of the binuclear center but is not caused by the absorbance of the radical itself since the strong heme absorbance would entirely mask the tyrosine radical signal. It is not unlikely that the closeness of the tyrosine radical to cytochrome a_3 and Cu_B could significantly affect their spectra (*40*).

A third possibility also accounting for the 1:1 mixture of the 607 nm and the 580 nm species while avoiding the reversal of the oxygen bond cleavage is a branching mechanism in which compound A decays into the 607 nm species and the F_o 580 nm species by two separate paths; subsequently both intermediates decay into F_I. In this case, the 607 nm species could either be a true peroxy structure or a ferryl with an oxidizing equivalent on the nearby tyrosine. Our data cannot distinguish between a sequential and a branching mechanism, but we favor the former.

Proton Uptake. A postulated uptake of protons, although not monitored in this study, is included in Scheme 1. Studies in our laboratory[3] and those of Hallén and co-workers have shown that proton uptake is associated with at least the 100 μs phase (*34*, *39*) and the 1 ms phase when the O_2-reduction reaction is monitored in the presence of a pH-sensitive dye. Accordingly, a proton is postulated to be taken up during the decay of intermediate F_o to F_I and during the conversion of F_{II} to intermediate 6. If the 607 nm intermediate is indeed a ferryl with an oxidizing equivalent on tyrosine 244, the cleavage of the O−O bond would be expected to be facilitated by protonation at the binuclear center. In Scheme 1, tyrosine 244 is proposed to function both as an electron and proton donor, transferring a hydrogen atom to the binuclear center during the O−O bond cleavage. Proton uptake during the formation of intermediate 4 is supported by results of Hallén and co-workers (*34*), which showed that this process, although independent of pH, had an isotope effect of 1.4, which was attributed to internal proton motion to the binuclear center.

CONCLUSIONS

There is now substantial evidence from our time-resolved data both in the visible and Soret regions for the existence of intermediates, R*, R, compound A, and the 607 nm ferryl species during the reduction of O_2 to water. The excellent agreement between the model and experimental spectra of R, F_I, and F_{II} (Figures 6 and 9) in both regions supports this, and comparison of the spectra of compound A (Figure 7) to those of model compounds (*36*) strengthens the argument that the spectrum of compound A is correct. While there was reasonable agreement between intermediate 4 and that of the 607 nm species of cytochrome oxidase in the visible region (*11*), both with peaks of equal intensities centered at 606 nm in the difference spectrum referenced versus the oxidized enzyme, the data in the Soret region did not support this model unless one assumed significant spectral interactions. However, if intermediate 4 is a 1:1 mixture of the 607 nm species and the ferryl (580 nm), with cytochrome *a* reduced in the former, but oxidized in the latter, an excellent fit to intermediate 4 is observed in the Soret region (Figure 8c). A good fit is also obtained in the visible region using this combination (Figure 8d). Therefore, although the visible region was instrumental in determining the order of intermediates in the reaction of fully reduced cytochrome *c* oxidase with dioxygen (*11*), the additional information provided by analysis of the Soret data is required to provide a more complete mechanism, specifically with regard to the nature of intermediate 4.

ACKNOWLEDGMENT

We thank Professor Gerald Babcock for helpful discussions.

REFERENCES

1. Varotsis, C., Woodruff, W. H., and Babcock, G. T. (1989) *J. Am. Chem. Soc. 111*, 6439−6440.
2. Ogura, T., Takahashi, S., Shinzawa-Itoh, K., Yoshikawa, S., and Kitagawa, T. (1990) *J. Am. Chem. Soc. 112*, 5630−5631.
3. Han, S., Ching, Y.-C., and Rousseau, D. L. (1990) *Proc. Natl. Acad. Sci. U.S.A. 87*, 2491−2495.
4. Han, S., Ching, Y.-C., and Rousseau, D. L. (1990) *Nature 348*, 89−90.
5. Varotsis, C., and Babcock, G. T. (1990) *Biochemistry 29*, 7357−7362.
6. Ogura, T., Takahashi, S., Shinzawa-Itoh, K., Yoshikawa, S., and Kitagawa, T. (1990) *J. Biol. Chem. 265*, 14721−14723.
7. Varotsis, C., Zhang, Y., Appleman, E. H., and Babcock, G. T. (1993) *Proc. Natl. Acad. Sci. U.S.A. 90*, 237−241.
8. Babcock, G. T., and Wikström, M. (1992) *Nature 356*, 301−309.
9. Verkhovsky, M. I., Morgan, J. E., and Wikström, M. (1994) *Biochemistry 33*, 3079−3086.
10. Morgan, J. E., Verkhovsky, M. I., and Wikström, M. (1996) *Biochemistry 35*, 12235−12240.
11. Sucheta, A., Georgiadis, K. E., and Einarsdóttir, Ó. (1997) *Biochemistry 36*, 554−565.
12. Wikström, M., and Morgan, J. E. (1992) *J. Biol. Chem. 267*, 10266−10273.
13. Bickar, D., Bonaventura, J., and Bonaventura, C. (1982) *Biochemistry 21*, 2661−2666.
14. Wrigglesworth, J. M. (1984) *Biochem. J. 217*, 715−719.
15. Vygodina, T. V., and Konstantinov, A. A. (1988) *Ann. N. Y. Acad. Sci. 550*, 124−138.
16. Fabian, M., and Palmer, G. (1995) *Biochemistry 34*, 13802−13810.
17. Orii, Y. (1988) *Ann. N.Y. Acad. Sci. 550*, 105−117.
18. Konstantinov, A. A., Capitanio, N., Vygodina, T. V., and Papa, S. (1992) *FEBS Lett. 312*, 71−74.
19. Verkhovsky, M. I., Morgan, J. E., and Wikström, M. (1996) *Proc. Natl. Acad. Sci. U.S.A. 93*, 12235−12239.
20. Weng, L., and Baker, G. M. (1991) *Biochemistry 30*, 5727−5733.
21. Ogura, T., Hirota, S., Proshlyakov, D. A., Shinzawa-Itoh, K., Yoshikawa, S., and Kitagawa, T. (1996) *J. Am. Chem. Soc. 118*, 5443−5449.
22. Blair, D. F., Witt, S. N., and Chan, S. I. (1985) *J. Am. Chem. Soc. 107*, 7389−7399.
23. Witt, S. N., and Chan, S. I. (1987) *J. Biol. Chem. 262*, 1446−1448.
24. Ferguson-Miller, S., and Babcock, G. T. (1996) *Chem. Rev. 96*, 2889−2907.
25. Bose, S., Hendler, R. W., Shrager, R. I., Chan, S. I., and Smith, P. D. (1997) *Biochemistry 36*, 2439−2449.
26. Yoshikawa, S., Choc, M. G., O'Toole, M. C., and Caughey, W. S. (1977) *J. Biol. Chem. 252*, 5498−5508.
27. Georgiadis, K. E., Jhon, N.-I., and Einarsdóttir, Ó. (1994) *Biochemistry 33*, 9245−9256.
28. Einarsdóttir, Ó., Georgiadis, K. E., and Sucheta, A. (1995) *Biochemistry 34*, 496−508.
29. Slutter, C. E., Sanders, D., Wittung, P., Malmström, B. G., Aasa, R., Richards, J. H., Gray, H. B., and Fee, J. A. (1996) *Biochemistry 35*, 3387−3395.
30. Fabian, M., and Palmer, G. (1995a) *Biochemistry 34*, 1534−1540.
31. Vanneste, W. H. (1966) *Biochemistry 5*, 838−848.
32. Ogura, T., Yoshikawa, S., and Kitagawa, T. (1985) *Biochemistry 24*, 7746−7752.
33. Oliveberg, M., Brzezinski, P., and Malmström, B. G. (1989) *Biochim. Biophys. Acta 977*, 322−328.
34. Hallén, S., and Nilsson, T. (1992) *Biochemistry 31*, 11853−11859.
35. Einarsdóttir, Ó., Dyer, R. B., Lemon, D. D., Killough, P. M., Hubig, S. M., Atherton, S. J., López-Garriga, J. J., Palmer, G., and Woodruff, W. H. (1993) *Biochemistry 32*, 12013−12024.
36. Babcock, G. T., and Chang, C. K. (1979) *FEBS Lett. 97*, 358−362.
37. Yoshikawa, S., Shinzawa-Itoh, K., Nakashima, R., Yaone, R., Yamashita, E., Inoue, N., Yao, M., Fei, M. J., Libeu, C. P., Mitzushima, T., Yamaguchi, H., Tomizaki, T., and Tsukihara, T. (1998) *Science 280*, 1723−1731.
38. Ostermeier, C., Harrenga, A., Ermler, U., and Michel, H. (1997) *Proc. Natl. Acad. Sci. U.S.A. 94*, 10547−10553.
39. Oliveberg, M., Hallén, S., and Nilsson, T. (1991) *Biochemistry 30*, 436−440.
40. Proshlyakov, D. A., Pressler, M. A., and Babcock, G. T. (1998) *Proc. Natl. Acad. Sci. U.S.A. 95*, 8020−8025.
41. Kobayashi, K., Une, H., and Hayashi, K. (1989) *J. Biol. Chem. 264*, 7976−7980.
42. Nilsson, T. (1992) *Proc. Natl. Acad. Sci. U.S.A. 89*, 6497−6501.
43. Geren, L. M., Beasley, J. R., Fine, B. R., Saunders, A. J., Hibdon, S., Pielak, G. J., Durham, B., and Millet, F. (1995) *J. Biol. Chem. 270*, 2466−2472.
44. Morgan, J. E., Li, P. M., Jang, D.-J., El-Sayed, M. A., and Chan, S. I. (1989) *Biochemistry 28*, 6975−6983.
45. Oliveberg, M., and Malmström, B. G. (1991) *Biochemistry 30*, 7053−7057.
46. Verkhovsky, M. I., Morgan, J. E., and Wikström, M. (1992) *Biochemistry 31*, 11860−11863.
47. Hallén, S., and Brzezinski, P. (1994) *Biochim. Biophys. Acta 1184*, 207−218.
48. Ramirez, B. E., Malmström, B. G., Winkler, J. R., and Gray, H. B. (1995) *Proc. Natl. Acad. Sci. U.S.A. 92*, 11949−11951.
49. Proshlyakov, D. A., Ogura, T., Shinzawa-Itoh, K., Yoshikawa, S., Appelman, E. H., and Kitagawa, T. (1994) *J. Biol. Chem. 269*, 29385−29388.
50. Proshlyakov, D. A., Ogura, T., Shinzawa-Itoh, K., Yoshikawa, S., and Kitagawa, T. (1996) *Biochemistry 35*, 76−82.
51. Proshlyakov, D. A., Ogura, T., Shinzawa-Itoh, K., Yoshikawa, S., and Kitagawa, T. (1996) *Biochemistry 96*, 8580−8586.

BI981092W